MOLECULAR AND CELLULAR BIOLOGY, Apr. 2007, p. 3123–3130 Vol. 27, No. 8
0270-7306/07/$08.00+0 doi:10.1128/MCB.01188-06

Early Embryonic Lethality of Mice Lacking the Essential Protein SNEV▽‡

Klaus Fortschegger,[1] Bettina Wagner,[2]† Regina Voglauer,[1] Hermann Katinger,[1] Maria Sibilia,[2,3] and Johannes Grillari[1]*

Institute of Applied Microbiology, Department of Biotechnology, University of Natural Resources and Applied Life Sciences, A-1190 Vienna, Austria,[1] and Department of Dermatology, Division of Immunology, Allergy and Infectious Diseases, Medical University of Vienna,[2] and Competence Center for Biomolecular Therapeutics,[3] A-1090 Vienna, Austria

Received 30 June 2006/Returned for modification 10 August 2006/Accepted 27 January 2007

SNEV (Prp19, Pso4, NMP200) is a nuclear matrix protein known to be involved in pre-mRNA splicing, ubiquitylation, and DNA repair. In human umbilical vein endothelial cells, SNEV overexpression delayed the onset of replicative senescence. Here we analyzed the function of the mouse *SNEV* gene in vivo by employing homologous recombination in mice and conclude that SNEV is indispensable for early mouse development. Mutant preimplantation embryos initiated blastocyst formation but died shortly thereafter. Outgrowth of *SNEV*-null blastocysts showed a lack of proliferation of cells of the inner cell mass, which subsequently underwent cell death. While *SNEV*-heterozygous mice showed no overt phenotype, heterozygous mouse embryonic fibroblast cell lines with reduced SNEV levels displayed a decreased proliferative potential in vitro. Our experiments demonstrate that the SNEV protein is essential, functionally nonredundant, and indispensable for mouse development.

SNEV, also known as Prp19, Pso4, or NMP200, is a ubiquitously expressed, highly conserved nuclear matrix protein of 56 kDa and is involved in diverse pathways, such as pre-mRNA splicing (13) and DNA repair (25). Furthermore, SNEV also displays E3 ubiquitin ligase activity in vitro (15, 17). Although it is not an integral part of small nuclear ribonucleoproteins, Prp19 is required for the formation of an activated spliceosomal complex in *Saccharomyces cerevisiae* (6, 13, 31) by specifying the interaction of U5 and U6 with pre-mRNA (5, 26). The proteins of the Prp19-associated complex (31), which is also called the nineteen complex in yeast or the CDC5L complex in humans (1), and their interactions seem to be conserved in budding and fission yeasts, mammals (20), and even plants (40). Previously we have shown that SNEV is downregulated in senescent human umbilical vein endothelial cells (HUVECs) (14) and that its overexpression leads to an extension of the cellular life span, which correlates with an enhanced stress resistance (39). SNEV is upregulated after exposure to genotoxic agents and seems to be involved in the repair of DNA double-strand breaks and interstrand cross-links (25, 44). Very recent findings even indicate that mouse SNEV might be involved in lipid droplet biogenesis (7). Additionally, SNEV seems to play an important role in brain development and function, since it was shown to be gradually downregulated in the hippocampi of patients with Alzheimer's disease (2), and a slightly different splice variant of mouse SNEV might be involved in neuronal/astroglial cell fate decisions (38).

SNEV consists of an N-terminal U-box domain, which is a modified RING finger typical of a new class of ubiquitin E3 ligases (17) that interacts with the proteasome (24), and of seven C-terminal WD40 repeats, which are known to mediate protein-protein interactions (35). The E3 ligase activity might be important for splicing and/or DNA repair by mediating rearrangements through ubiquitylation and degradation of yet-unknown targets by the proteasome (24). In between these domains lies a low-complexity coiled-coil region, which is responsible for the tetramerization of yeast Prp19 (31) as well as for the interaction with other proteins of the nineteen complex (30, 31). Apart from its already known interaction with the spliceosome, a smaller CDC5L complex containing CDC5L, SNEV, PLRG1, and SPF27 was recently found to interact with the helicase/endonuclease WRN (44), a protein involved in DNA repair and telomere maintenance. Mutations of *WRN* are responsible for a segmental progeroid hereditary disorder also known as Werner syndrome (3). Thus, being an essential component of the CDC5L complex, SNEV represents an interesting new link between pre-mRNA splicing, ubiquitylation, and DNA repair (18).

In order to better understand the biological function of SNEV, gene targeting was employed to inactivate the *SNEV* gene in mice. In this report, we show that heterozygous mice display no obvious phenotype and that males as well as females are fertile and transmit the null allele to their progeny. Nullizygous offspring were never obtained from $SNEV^{+/-}$ intercrosses, indicating that the deletion of *SNEV* is embryonic lethal in mice. SNEV-deficient embryos were not observed at postimplantation stages. However, knockout blastocysts could be recovered at 3.5 days postcoitus (dpc) and displayed increased cell death and severe defects in the outgrowth capacity of the inner cell mass (ICM). Furthermore, heterozygous mouse embryonic fibroblasts (MEFs) with decreased SNEV levels stop proliferation earlier than controls in vitro. Since the important function of SNEV in pre-mRNA splicing has been described, we speculate that the absence of SNEV affects the

* Corresponding author. Mailing address: Institute of Applied Microbiology, Muthgasse 18, A-1190 Vienna, Austria. Phone: 431360066230. Fax: 4313697615. E-mail: johannes.grillari@boku.ac.at.

† Present address: Apeiron Biologics, A-1230 Vienna, Austria.

‡ Supplemental material for this article may be found at http://mcb.asm.org/.

▽ Published ahead of print on 5 February 2007.

pre-mRNA splicing complex, thereby severely impairing the survival and proliferation of *SNEV*-deficient cells and embryos.

MATERIALS AND METHODS

Analysis of the *SNEV* mRNA and gene sequences. Starting from the mRNA sequence of human SNEV, degenerate primers were designed for amplification of a murine open reading frame from NIH 3T3 cells. One of these amplification products was employed as a probe for screening of the mouse BAC library I (strain 129/SvJ) by Incyte Genomics. The insert DNA of the obtained positive clone 240/H13 was successively sequenced (I.B.L., Austria), and the resulting trace data were aligned with DNA-Star software. The sequence information was submitted to GenBank and utilized for the cloning of the targeting vector. After release of the whole-genome sequences of mouse, rat, and human, the corresponding genomic regions were aligned and compared with the online tool VISTA, using default parameters (8).

Gene-targeting construct and homologous recombination in ES cells. A 5-kb 5′-end-homologous region containing the promoter and a 1-kb 3′-end-homologous region containing exons 7 and 8 of *SNEV* were cloned into the conventional replacement vector pGNA (34). This plasmid also contained a neomycin resistance cassette for positive selection, the cell-autonomous diphtheria toxin fragment A (DTA) cassette for negative selection, and a *lacZ* reporter gene. Twenty-five micrograms of the SmaI-linearized targeting construct was electroporated into 2×10^7 HM-1 embryonic stem (ES) cells. The cells were then cultured in ES cell medium (Dulbecco's modified Eagle's medium containing 4.5 g/liter glucose, 100 μM nonessential amino acids, 0.1 mM β-mercaptoethanol, 2 mM L-glutamine, 50 U/ml penicillin, 50 μg/ml streptomycin, 15% fetal bovine serum, and 1,000 U/ml leukemia inhibitory factor) supplied with 350 μg/ml G418 (Invitrogen). After 1 week, resistant clones were picked, and half of each clone was lysed with 12 μl lysis buffer (34) (1× Gitschier's buffer, 1.7 μM sodium dodecyl sulfate, 50 μg/ml proteinase K) and screened for homologous recombinants by nested PCR. In the first PCR, primers NeoSI and 3′ASI were used, while in the second reaction, primers NeoSII and 3′ASII were employed for PCR (for primer sequences, see Table S1 in the supplemental material). The amplification was done in standard PCR buffer containing 200 nM of each primer, 200 μM of each deoxynucleoside triphosphate, and 2 U *Taq* polymerase (Sigma) under the following conditions: 97°C for 1 min and 35 cycles of 94°C for 30 s, 57°C for 30 s, and 72°C for 2 min. Positive cell clones were expanded, and the recombination event was confirmed by Southern blotting of genomic DNA digested with NcoI or XhoI (New England Biolabs). Restriction fragments were separated by electrophoresis on a 0.7% agarose gel, alkaline blotted to a positively charged nylon membrane (Roche), and hybridized at 65°C in Church buffer to an 800-bp [^{32}P]dCTP-labeled probe (Amersham Megaprime kit) recognizing a sequence in the *SNEV* locus downstream of the 3′-end-homologous region. After being washed, the blots were exposed to BioMax MS film (Kodak) for 5 days.

Generation of knockout mice. ES cells heterozygous for the *SNEV* deletion were injected into C57BL/6 blastocysts, which were then implanted into pseudopregnant foster mothers. High-contribution chimeras were obtained, some of which also transmitted the targeted allele through the germ line. Since mice of a pure 129/Sv background were poor breeders, heterozygous mice were backcrossed to C57BL/6 mice and kept in a 129/Sv × C57BL/6 background. All of the following experiments were therefore performed with mice of a mixed 129/Sv × C57BL/6 genetic background. Mice were genotyped by a three-primer PCR using mouse tail DNA as a template and the primers 3′SI, NeoSI, and 3′ASI, which allows the discrimination between the wild-type and the targeted allele. Approximately 100 ng of DNA was used for amplification according to the same PCR protocol described above. All mice were held in accordance with institutional policies and federal guidelines.

Isolation and genotyping of mouse embryos. For analysis of postimplantation embryos, $SNEV^{+/-}$ females were sacrificed at defined time points (see Table 1) after being mated to heterozygous stud males. Embryos were dissected from the uteri and yolk sacks and washed in phosphate-buffered saline (PBS), and DNA was isolated after proteinase K (Roche) digestion. Genotyping was performed by the three-primer PCR mentioned above. For blastocyst outgrowths, heterozygous 4- to 7-week-old female mice were superovulated by intraperitoneal injection of pregnant mare's serum (5 IU per animal) and, 48 h later, human chorionic gonadotropin (5 IU per animal) and were subsequently mated with $SNEV^{+/-}$ males. Plugged females were euthanized, and their uteri were dissected and flushed with ES cell medium at 3.5 dpc. Single blastocysts were seeded onto gelatinized 96-well plates containing 200 μl medium and incubated at 37°C with 5% CO_2. After 4 days, the medium was changed, and after 7 days in culture, blastocyst DNA was isolated (29). Separate nested PCRs were performed with the primers NeoSI and 3′ASI in the first reaction and the primers NeoSII and 3′ASIII in the second reaction for the targeted allele and with the primers 3′SI and 3′ASI in the first reaction and the primers 3′SIII and 3′ASIII in the second reaction for the wild-type allele. PCR conditions were again the same as those described above.

TUNEL and indirect immunofluorescence of blastocyst outgrowths. Blastocysts were isolated at 3.5 dpc, seeded onto fibronectin-coated eight-well chamber slides (Nalgene Lab-Tek) filled with 200 μl ES cell medium, incubated at 37°C with 5% CO_2 for 4 days, washed with PBS, fixed with 3% paraformaldehyde in PBS for 30 min at room temperature, treated with ice-cold 0.1% Triton X-100 in 0.1% sodium citrate buffer for 5 min, and incubated with 50 μl terminal deoxynucleotidyltransferase-mediated dUTP-fluorescein nick end labeling assay (TUNEL) reaction mix (in situ cell death detection kit with fluorescein; Roche) at 37°C for 2 h. After being washed with PBS, the slides were counterstained with 2.5 μg/ml propidium iodide. The genotypes were determined by nested PCR. For indirect immunofluorescence staining for SNEV and 5-bromo-2′-deoxyuridine (BrdU), blastocysts were grown for 4 days as described above and incubated with 10 μM BrdU overnight. After fixation with ice-cold 70% ethanol, denaturation/permeabilization with 2 M HCl–0.5% Triton X-100, and neutralization, cells were incubated with mouse anti-BrdU (1:2; Becton Dickinson) and rabbit anti-Prp19 (1:50, No867, kindly provided by Paul Ajuh) antibodies. Secondary antibodies were anti-mouse immunoglobulin G (IgG)–fluorescein isothiocyanate and anti-rabbit IgG–tetramethyl rhodamine isothiocyanate (1:100 and 1:50, respectively; both from Sigma). The slides were analyzed on a Leica TCS SP2 confocal microscope. Since the PCR was not compatible with the acid denaturation in the BrdU experiment, here the *SNEV*-null genotype was deduced from the weak SNEV signal and the previously observed altered appearance.

Isolation and cultivation of MEFs. Embryos of the 129/Sv × C57BL/6 background were dissected at 13.5 dpc, the heads and livers were removed, and genotypes were determined by the three-primer PCR. The remaining tissues were minced by repeated pipetting in 0.25% trypsin in PBS; they were supplied with Dulbecco's modified Eagle's medium (Biochrom), 10% fetal calf serum, 4 mM L-glutamine, 50 U/ml penicillin, and 50 μg/ml streptomycin and centrifuged, and 3×10^5 cells were seeded per gelatinized T25 Roux flask. The cultures were incubated at 37°C with 7% CO_2 and passaged two times a week according to the 3T3 protocol (37).

Northern blotting and qRT-PCR. For total RNA preparation, MEF cells were pelleted, washed with PBS, and resuspended in 1 ml TRIzol reagent (Invitrogen), and RNA was isolated according to the manufacturer's protocol. For the quantitative real-time PCR (qRT-PCR), 2.5 μg total RNA was reverse transcribed with 200 U Superscript III reverse transcriptase (Invitrogen) and 500 ng of the oligo$(dT)_{18}$ primer at 50°C; the resulting cDNA was purified (QIAquick kit; QIAGEN) and eluted in 100 μl elution buffer. PCR was performed on a Rotor-Gene 2000 cycler (Corbett Research) with Platinum SYBR green qPCR SuperMix-UDG (Invitrogen) and primers at a 250 nM final concentration (for qRT primer sequences, see Table S1 in the supplemental material). The temperature profile was 50°C for 2 min; 95°C for 2 min; and 40 cycles of 94°C for 10 s, 55°C for 15 s, 72°C for 15 s and 80°C for 5 s (fluorescence data acquisition). The absence of primer dimers and genomic PCR products was confirmed by subsequent melt curve analysis. Standard curves were obtained for each run in duplicates by amplification of five serial 1:10 dilutions of the corresponding quantified PCR product, and 1 μl of the individual cDNA sample was amplified in triplicates. Relative quantification was performed by normalizing the target gene copy numbers for SNEV, p16, and PAI-1 to those of glyceraldehyde-3-phosphate dehydrogenase (GAPDH) and β-actin (ACTB). For Northern blot analysis, 10 μg of each total RNA was separated on a denaturing formaldehyde gel containing 1% agarose and blotted onto nylon membranes using 10× SSC (1× SSC is 0.15 M NaCl plus 0.015 M sodium citrate). The blots were hybridized at 65°C in Church buffer to [^{32}P]dCTP-labeled probes comprising the entire 1,500-bp open reading frame of the murine SNEV protein or the 140-bp qRT-PCR product of mouse β-actin.

Western blotting. MEF cells were lysed with DIGE lysis buffer {30 mM Tris, 7 M urea, 2 M thiourea, 4% 3-[(3-cholamidopropyl)-dimethylammonio]-1-propanesulfonate (CHAPS; pH 8.5)}, and protein concentration was measured with the 2-D Quant kit (Amersham). Sodium dodecyl sulfate-polyacrylamide gel electrophoresis with these lysates (10 μg total protein per lane) was performed on NuPage 4 to 12% gels (Invitrogen) and blotted onto a polyvinylidene difluoride membrane (Millipore). Blots were blocked with 3% bovine serum albumin and 0.1% Tween 20 in PBS and incubated with a rabbit anti-SNEV antibody (1:2,500, No866, kindly provided by Paul Ajuh), anti-rabbit IgG–peroxidase (1:5,000; Sigma), and ECL-Plus (Amersham) for the analysis of SNEV and with mouse anti-β-actin (1:10,000; Sigma), anti-mouse IgG–alkaline phosphatase (1:

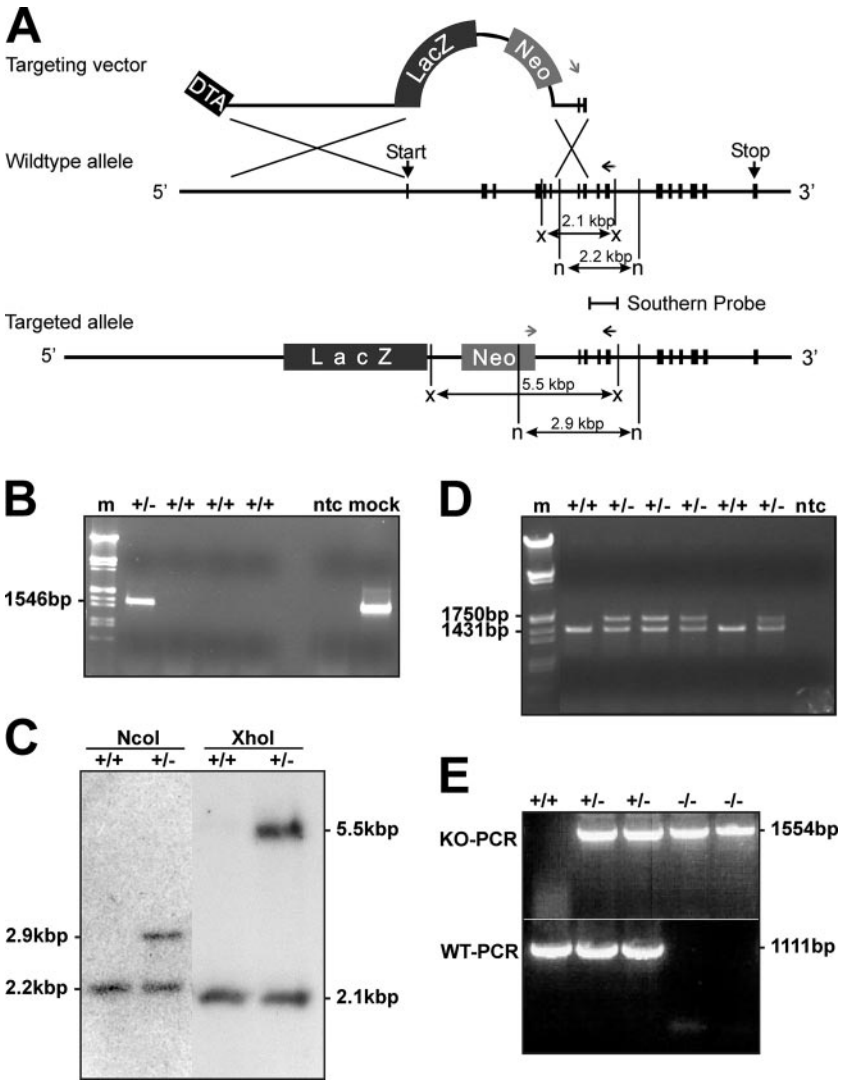

FIG. 1. Targeted disruption of the murine *SNEV* locus. (A) Homologous recombination of the targeting construct with the wild-type locus leads to a loss-of-function targeted allele. Small boxes indicate exons; the start and stop codons lie in the first and last exons, respectively. The first six exons were replaced by a *lacZ* reporter (LacZ) and a neomycin resistance cassette (Neo), both containing poly(A) signals and the latter also carrying a Rous sarcoma virus promoter. The DTA cassette was used as a negative selection marker. Restriction sites for NcoI (n) and XhoI (x) and PCR screening primer binding sites (short arrows) are shown. (B) Nested PCR screening of representative ES cell clones yielded a 1,546-bp product, if the locus was correctly targeted. m, marker lane; ntc, no template negative control; mock, mock vector positive control. (C) Southern blotting using a radioactively labeled probe was performed to confirm the correct integration of the targeting construct. Digestion with restriction enzyme NcoI or XhoI yields fragments of 2.9 and 5.5 kbp for the targeted allele and 2.2 and 2.1 kbp for the wild-type allele, respectively. (D) Genotyping of mice and embryos by a three-primer PCR yielded a product of 1,750 bp for the knockout allele and one of 1,431 bp for the wild-type allele. (E) Genotyping of blastocysts by nested PCR. Amplification with wild-type primers (WT-PCR) yielded a 1,111-bp product for the wild-type allele. With neomycin-specific sense primers, a product of 1,554 bp was amplified from the targeted allele (knockout [KO]-PCR).

5,000; Sigma), and CDP-Star (NEB) for the housekeeping gene. Chemiluminescence signal detection was performed on a Lumi-Imager (Roche). For quantification, protein was blotted to a nitrocellulose membrane (Millipore), incubated with anti-SNEV and anti-β-actin as primary antibodies and anti-mouse Alexa680 (Invitrogen) and anti-rabbit IRdye800 (Rockland) as secondary antibodies (1:5,000 each), scanned, and relatively quantified using an Odyssey scanner (LI-COR).

Nucleotide sequence accession numbers. The following nucleotide sequences were deposited in GenBank under the accession numbers given: the *Homo sapiens* SNEV (Prp19, Prpf19, hPso4, hNMP200) mRNA, NM_014502; the *H. sapiens SNEV* gene, GeneID 27339; the *Rattus norvegicus SNEV* gene, GeneID 246216; the *Mus musculus* SNEV mRNA, AF251503 (submitted), NM_134129 (curated); and the *M. musculus SNEV* gene, AF386760 (submitted), GeneID 28000 (curated).

RESULTS

Sequence analysis of the murine *SNEV* locus. We identified SNEV as a multifunctional protein taking part in different important cellular functions. To investigate its role in vivo, we disrupted the *SNEV* gene in mice. Therefore, we cloned the mouse gene by screening an isogenic 129/SvJ genomic BAC clone library with a SNEV mRNA sequence derived from NIH 3T3 cells. The nucleotide sequence of the 2.1-kb mRNA as well as that of the 16.5-kb genomic locus comprising all 16 exons, introns, and the surrounding regions were submitted to the GenBank database. Sequence

TABLE 1. Genotypes of *SNEV*$^{+/-}$ intercross progeny produced in this study

Age (dpc)	No. (%) of mice with indicated genotype			No. (%) of resorptions[a]	Total
	+/+	+/−	−/−		
Newborn	118 (37)	198 (63)	0 (0)	NA	316
10.5–13.5	6 (13)	18 (39)	0 (0)	22 (48)	46
7.5–9.5	8 (20)	18 (45)	0 (0)	14 (35)	40
3.5	27 (27)	55 (57)	7 (8)	7 (8)[b]	96

[a] NA, not applicable.
[b] No growth or genotype not detectable.

comparison showed a high degree of similarity between the *Mus musculus* locus and the corresponding gene sequences of *Homo sapiens* and *Rattus norvegicus*, especially regarding the lengths and sequences of the exons (see Fig. S1 in the supplemental material). The amino acid sequences of the translated proteins are even more conserved (>99% similarity).

Targeted disruption of the *SNEV* gene. The pGNA-based targeting vector containing a long 5′-end and a short 3′-end homology arm was electroporated into mouse ES cells. Homologous recombination at the *SNEV* locus resulted in replacement of the first six exons of *SNEV* by the *lacZ* reporter and the neomycin resistance cassette (Fig. 1A). Random integration was reduced by the presence of a DTA cassette at the 5′ end of the targeting construct (27). A total of 6 out of 232 neomycin-resistant ES clones were correctly targeted (2.5% efficiency), as confirmed by nested PCR (Fig. 1B) and Southern blotting (Fig. 1C) at the 3′-end-flanking region. Heterozygous ES cell clones were injected into C57BL/6 blastocysts, and two of them formed germ line chimeras, which transmitted the targeted allele to their offspring. Heterozygous *SNEV*$^{+/-}$ mice of a 129/Sv or mixed 129/Sv × C57BL/6 background identified by PCR (Fig. 1D) were viable and fertile. In comparison with control littermates, they did not exhibit any overt phenotype, had similar body and organ weights (see Fig. S2 in the supplemental material), and had a normal median life span of more than 18 months. *SNEV*-heterozygous mice were intercrossed to

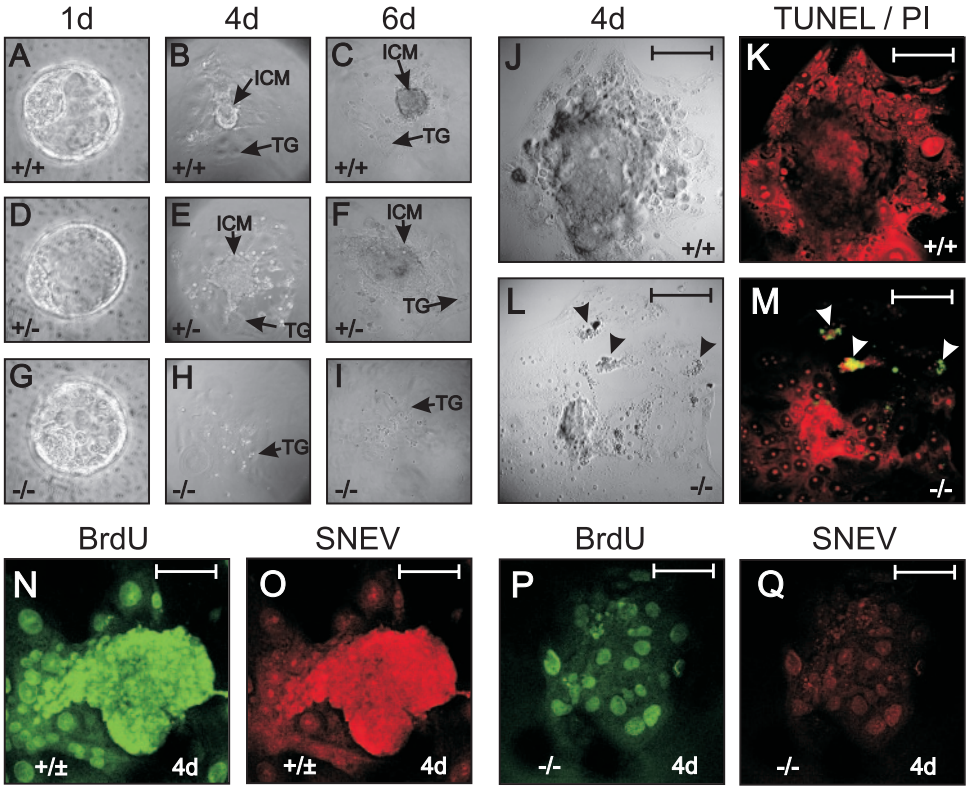

FIG. 2. Nullizygous blastocysts fail to grow in vitro. Blastocysts were isolated from *SNEV*$^{+/-}$ intercrosses at 3.5 dpc and cultured in ES cell medium for 1 week. Phase-contrast pictures of one representative +/+ (A to C), +/− (D to F), or −/− (G to I) blastocyst each on days 1 (A, D, G), 4 (B, E, H), and 6 (C, F, I) after isolation are shown. Trophoblastic giant cells (TG) surround the ICM, which disappears with time in *SNEV*$^{-/-}$ blastocysts. Pictures at day 1 were taken with a 20× lens objective and at days 4 and 6 with a 10× lens objective. Microphotographs (J, L) and images after cell death detection staining (K, M) with dUTP-fluorescein (green) and propidium iodide (PI) (red). While wild-type blastocysts develop normally (J, K), the ICMs of nullizygous blastocysts decrease at day 4 and cells (arrowheads) begin to form vesicles (L) and stain positively by TUNEL (M). The genotypes of the blastocysts were determined by nested PCR. (N to Q) Indirect immunofluorescence. Blastocysts, which grew out for 4 days and were incubated with BrdU overnight, were stained for SNEV (red) and BrdU (green). While the control displays high BrdU incorporation (N) and normal SNEV levels (O), the putative *SNEV*-null outgrowth has already lost ICM and stains only weakly for BrdU (P) and SNEV (Q) in trophoblasts. In this case, the absence of the SNEV allele was deduced from the weak SNEV signal and the altered appearance. Bars, 100 μm.

obtain *SNEV*-nullizygous mice. However, no $SNEV^{-/-}$ pups could be identified among over 300 analyzed offspring, either in the inbred 129/Sv or in the mixed 129/Sv × C57BL/6 background groups, suggesting that the deletion of *SNEV* leads to embryonic lethality. In contrast, $SNEV^{+/+}$ and $SNEV^{+/-}$ mice were obtained at the Mendelian frequency (Table 1).

***SNEV*$^{-/-}$ embryos die at the blastocyst stage.** In order to determine the developmental stage when *SNEV*-null fetuses die, embryos derived from $SNEV^{+/-}$ intercrosses were genotyped at different stages of gestation (Table 1). Since no nullizygous embryos but many resorptions were observed after implantation between 7.5 and 13.5 dpc, we concluded that $SNEV^{-/-}$ embryos might die at the preimplantation or early postimplantation stage. Therefore, around 100 blastocysts were isolated at 3.5 dpc and cultured singularly in vitro for 1 week under daily observation. PCR analysis revealed that approximately 7 to 8% of the blastocyst outgrowths were $SNEV^{-/-}$ (Fig. 1E) but that another 7 to 8% gave no PCR amplification product. Presumably, the latter were originally also *SNEV*-null blastocysts but could no longer be genotyped because only very low cell numbers were present after 7 days in culture. Shortly after isolation, blastocysts were normal and indiscernible from those of controls (Fig. 2A, D, and G). Morphological inspection of the individual blastocyst cultures revealed that wild-type and $SNEV^{+/-}$ blastocysts differentiated correctly into trophectodermal giant cells and growing ICMs, hatched from their zonae pellucidae, and attached to the culture dish surface 2 to 3 days after being plated (Fig. 2B and E). $SNEV^{-/-}$ blastocysts also hatched, and their trophoblast cells attached to the culture surface and differentiated (Fig. 2H). However, unlike with the wild-type and heterozygous blastocysts (Fig. 2C and F), the cells in their ICMs did not proliferate, and after 6 days of culture, their overall cell numbers were dramatically decreased (Fig. 2I). TUNEL staining performed at different stages after plating revealed the presence of significantly higher numbers of dying, presumably apoptotic, cells in $SNEV^{-/-}$ blastocyst outgrowths starting around day 4 of culture (Fig. 2L and M), whereas wild-type outgrowths developed normally (Fig. 2J and K). While, at this stage, control blastocyst outgrowths proliferated strongly, as shown by BrdU incorporation (Fig. 2N), and had normal SNEV levels (Fig. 2O), in *SNEV*-deficient outgrowths, no proliferation in the ICMs could be detected. However, trophoblast giant cells of *SNEV*-null embryos stained weakly positive for both BrdU (Fig. 2P) and SNEV (Fig. 2Q), suggesting that endoreplication was still taking place to some extent. These results show that *SNEV*-deficient embryos are viable at the blastocyst stage but do not develop further after implantation, since the ICM undergoes cell death. Because of this severe phenotype, no *SNEV*-deficient cells could be obtained to perform further molecular investigations.

MEF cells with lowered SNEV levels have a decreased proliferative potential in vitro. We had previously observed that SNEV-overexpressing HUVECs have an increased life span (39). Therefore, we investigated whether there is also a difference in life span between murine wild-type and *SNEV*-heterozygous cells. MEFs were isolated from 13.5-dpc $SNEV^{+/+}$ and $SNEV^{+/-}$ fetuses and cultivated for at least 1 month according to the 3T3 protocol. SNEV mRNA expression levels were examined and compared to those of the housekeeping genes *ACTB* and *GAPD* by qRT-PCR (Fig. 3A) and Northern blotting (Fig. 3B). As expected, a twofold reduction in the amount of SNEV mRNA was observed in heterozygous cells compared to the level in wild-type MEFs. No additional band was detectable by Northern blot analysis (Fig. 3B); therefore,

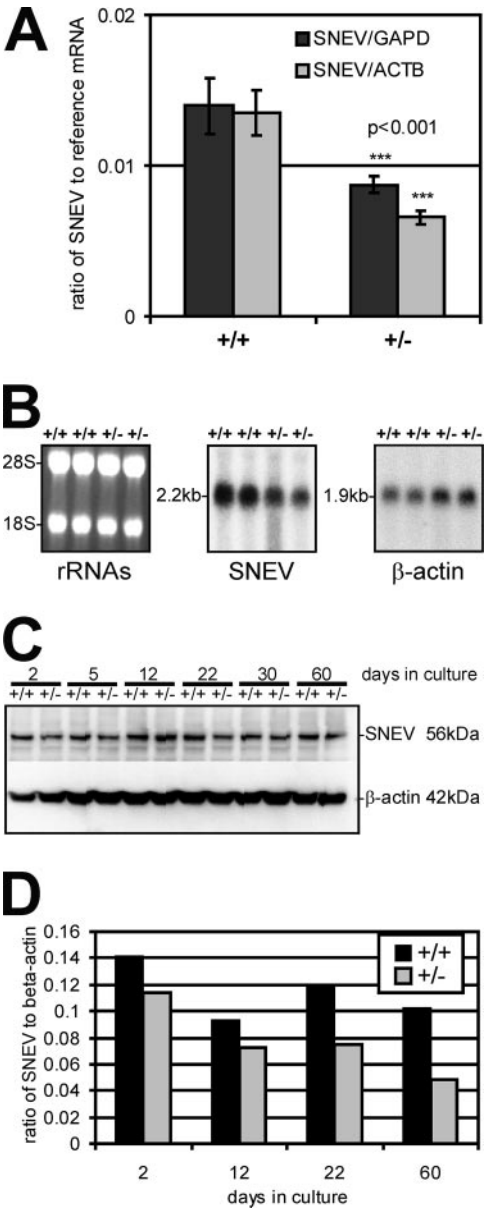

FIG. 3. Analysis of SNEV levels in MEFs. MEFs were isolated from 13.5-dpc embryos of $SNEV^{+/-}$ matings and cultivated according to the 3T3 protocol. (A) SNEV mRNA in +/+ and +/− cell lines was analyzed by qRT-PCR and normalized to housekeeping gene expression of GAPD (dark gray) and ACTB (light gray). SNEV mRNA levels in heterozygous cells were approximately 50% of those in wild-type cells. The difference was highly significant according to an unpaired *t* test. (B) Northern blots with probes against SNEV confirmed this result and showed no truncated transcript. Equal RNA loadings were controlled by rRNA band intensities and hybridization with a β-actin probe. (C) SNEV protein levels in one +/+ and one +/− cell line were analyzed by Western blotting at the cultivation time points shown in the figure. (D) SNEV protein levels were determined by scanning Western blots with an infrared scanner. SNEV levels in heterozygous MEFs were approximately 75% of those of wild-type cells and decreased with cultivation time.

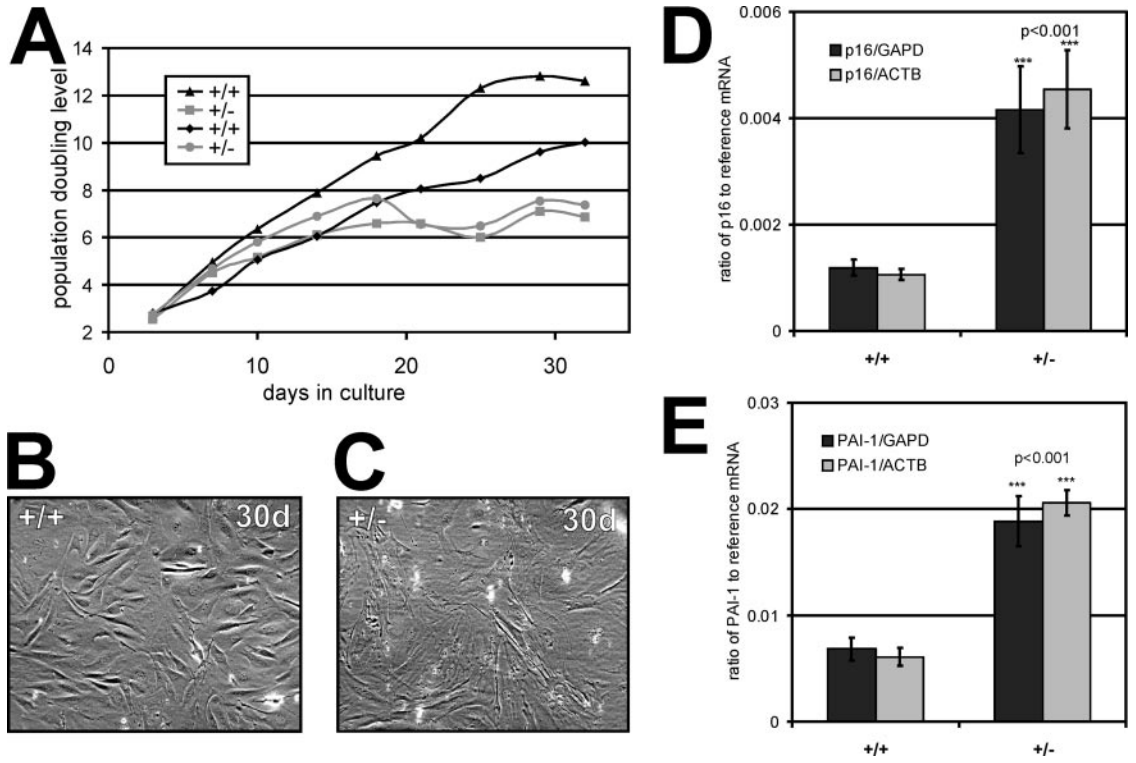

FIG. 4. Heterozygous MEFs have a decreased proliferative capacity. (A) Representative growth curves of two +/+ (black triangles and diamonds) and two +/− (gray circles and squares) cell lines. The population doubling level is plotted versus the number of days in culture. Most of the heterozygous cell lines had low SNEV levels and a decreased proliferative capacity in vitro. Heterozygous MEFs (C) display a senescence-like morphology after 30 days in culture, while wild-type (B) cells do this later. The p16 (D) and PAI-1 (E) mRNA levels of heterozygous MEFs cultivated for 30 days were significantly upregulated as determined by real-time PCR. Asterisks (D and E) indicate a highly significant difference according to an unpaired *t* test.

no aberrant transcripts were produced from the targeted allele. Western blot analysis revealed that heterozygous MEFs performing fewer population doublings contained on average 75% of the SNEV protein level of wild-type cells (Fig. 3C); furthermore, SNEV protein levels decreased slightly during cultivation (Fig. 3D), but the decrease was not as pronounced as that observed in HUVECs (14, 39).

In total, 30 MEF cell lines were established, and of these, 11 out of 17 $SNEV^{+/-}$ cell lines clearly had lower proliferative potentials than did 13 cell lines of wild-type littermate controls (representative examples are shown in Fig. 4A). The remaining six $SNEV^{+/-}$ cell lines did not show a decreased proliferation capacity but also had normal SNEV levels (data not shown), suggesting that cells which spontaneously express more SNEV or degrade it more slowly might overgrow the culture. After 30 days of cultivation, those heterozygous MEFs with lowered SNEV levels had stopped proliferation and displayed an enlarged and flattened morphology, like that of senescent fibroblasts (Fig. 4C), while cells of wild-type littermates looked like they did shortly after isolation (Fig. 4B). Additionally, this growth arrest was accompanied by the significant upregulation of the senescence markers $p16^{INK4a}$ (Fig. 4D) and PAI-1 (Fig. 4E) (22, 23), further strengthening the hypothesis that these MEFs reached senescence or a senescence-like state earlier than wild-type cells. We hypothesize that, while SNEV overexpression extends the life span and enhances the stress resistance of HUVECs (39), lower SNEV levels might lead to a higher susceptibility to oxidative stress, which seems to be the main cause for the replicative senescence of cultured murine fibroblasts (33).

These results demonstrate that, while a lowered SNEV protein level leads to an earlier growth arrest of MEFs in vitro, a complete lack of SNEV leads to the death of the ICM in blastocysts.

DISCUSSION

Here we report the effects on mouse development caused by the lack of the *SNEV* gene. SNEV is a protein highly conserved in *M. musculus*, *H. sapiens*, *R. norvegicus*, and yeast, where it is called Prp19 or Pso4 (13). SNEV is expressed in all human tissues tested and is constitutively expressed throughout the cell cycle (11). Moreover, it is expressed also in mouse oocytes and throughout early embryonic development (16, 43). SNEV is involved in pre-mRNA splicing, DNA repair, and ubiquitylation (15; see the Targeted Proteins Database, Current Biodata, Geneva, Switzerland). While mice heterozygous for *SNEV* do not show any overt phenotype, the inactivation of both *SNEV* alleles leads to early embryonic lethality around blastocyst implantation. Deletion of *PRP19* also leads to the lethality of *Saccharomyces cerevisiae*. Moreover, the thermosensitive yeast mutant strain *prp19-1* shows pleiotropic defects

in growth, sporulation, and forward mutability at nonpermissive temperatures (12). RNA interference-mediated knockdown of the homologue T10F2.4 in *Caenorhabditis elegans* also results in embryonic lethality (9, 21); in addition, the *Drosophila melanogaster* loss-of-function mutation $Prp19^{07838}$ is recessive lethal, and the respective embryos have clearly reduced numbers of hematopoietic crystal cells (28). Therefore, it seems that SNEV deficiency leads to lethality in diverse species throughout evolution, further strengthening the hypothesis that its function is essential and nonredundant.

SNEV might be indispensable for correct splicing; therefore, ICM cells will die due to a splicing defect comparable to the phenotypes of knockout mice for other general splicing factors, such as the SR domain proteins SRp20, ASF/SF2, and SC35 (19, 41, 42). Stalled splicing often leads to a block in transcription, as these two processes are tightly interconnected (10, 32, 36). Accordingly, in budding yeast, the thermosensitive mutant strain *prp19-1* accumulates pre-mRNA and decreases transcription levels when grown at nonpermissive temperatures (4).

It is well possible that in SNEV-deficient preimplantation mouse embryos, there is enough residual maternal SNEV protein and mRNA present to allow $SNEV^{-/-}$ embryos to reach the blastocyst stage, especially as the protein is quite stable. The high stability of the SNEV protein has been demonstrated for human cells; pulse-chase labeling experiments using Jurkat cells have shown that, after 24 h, there was still a high amount of labeled SNEV protein compared to amounts of other proteins, indicating that the turnover of SNEV is extremely low (11; C. Gerner, personal communication). However, once SNEV protein becomes limiting because of dilution and degradation, a block in pre-mRNA splicing and transcription will occur. As a consequence, unprocessed mRNA is restrained and degraded in the nucleus, cell division is blocked, and protein synthesis is stopped, subsequently leading to cell death. This situation most likely occurs in *SNEV*-deficient blastocysts. The amount of maternal SNEV mRNA and protein present in some *SNEV*-null blastocysts might be sufficient to reach the implantation stage in vivo and for trophoblast giant cells to survive and perform endoreplication after 4 days of outgrowth in vitro.

However, the possibility that the role of SNEV in DNA repair is also an essential, nonredundant function cannot be excluded. Deletions of important DNA repair genes, such as *ATR*, *Chk1*, *NBS1*, *BRCA1*, *BRCA2*, *Rad50*, *Rad51*, and *Mre11*, lead to early embryonic lethal phenotypes as well, which is attributed mainly to excessive p53-triggered apoptosis. As ICM cells are heavily affected by cell death in $SNEV^{-/-}$ blastocysts, it is possible that this is also due to defects in DNA repair. Since a more detailed analysis is prevented by the early lethality of *SNEV*-null cells and the insufficient knockdown effect of small interfering RNAs targeting SNEV, the exact underlying molecular events remain elusive. Interestingly, the recently discovered interaction of the CDC5L complex with the Werner helicase adds new possibilities of its involvement in DNA repair and telomere stability (44) and may account for the observed life span extension and increased stress resistance of SNEV-overexpressing HUVECs (39) and for the lowered proliferative potential of MEFs with decreased SNEV levels.

From our study, we can conclude that SNEV is indispensable for early mouse development and that it influences the proliferative potential of MEFs in vitro. Future experiments using stable RNA interference in different cell types or conditional knockout approaches using the Cre-*loxP* system may help to elucidate the exact in vivo function of the multifaceted protein SNEV.

ACKNOWLEDGMENTS

We thank Martina Hammer, Gertraud Steniczka, Kristin Baumann, Vera Gruber, and Tanja Miehl for their excellent technical assistance.

This work was kindly supported by Polymun Scientific, Austria, and by Austrian Science Fund grant NFN093-06. B.W. was the recipient of a DOC Fellowship of the Austrian Academy of Sciences. M.S. acknowledges support by the Competence Center for Biomolecular Therapeutics, by Austrian National Bank grant ÖNB-10556, and by EC program grant QLG1-CT-2001-00869.

REFERENCES

1. **Ajuh, P., B. Kuster, K. Panov, J. C. Zomerdijk, M. Mann, and A. I. Lamond.** 2000. Functional analysis of the human CDC5L complex and identification of its components by mass spectrometry. EMBO J. **19:**6569–6581.
2. **Blalock, E. M., J. W. Geddes, K. C. Chen, N. M. Porter, W. R. Markesbery, and P. W. Landfield.** 2004. Incipient Alzheimer's disease: microarray correlation analyses reveal major transcriptional and tumor suppressor responses. Proc. Natl. Acad. Sci. USA **101:**2173–2178.
3. **Bohr, V. A.** 2005. Deficient DNA repair in the human progeroid disorder, Werner syndrome. Mutat. Res. **577:**252–259.
4. **Burckin, T., R. Nagel, Y. Mandel-Gutfreund, L. Shiue, T. A. Clark, J. L. Chong, T. H. Chang, S. Squazzo, G. Hartzog, and M. Ares, Jr.** 2005. Exploring functional relationships between components of the gene expression machinery. Nat. Struct. Mol. Biol. **12:**175–182.
5. **Chan, S. P., and S. C. Cheng.** 2005. The Prp19-associated complex is required for specifying interactions of U5 and U6 with pre-mRNA during spliceosome activation. J. Biol. Chem. **280:**31190–31199.
6. **Chan, S. P., D. I. Kao, W. Y. Tsai, and S. C. Cheng.** 2003. The Prp19p-associated complex in spliceosome activation. Science **302:**279–282.
7. **Cho, S. Y., E. S. Shin, P. J. Park, D. W. Shin, H. K. Chang, D. Kim, H. H. Lee, J. H. Lee, S. H. Kim, M. J. Song, I. S. Chang, O. S. Lee, and T. R. Lee.** 2007. Identification of mouse Prp19p as a lipid droplet-associated protein and its possible involvement in the biogenesis of lipid droplets. J. Biol. Chem. **282:**2456–2465.
8. **Frazer, K. A., L. Pachter, A. Poliakov, E. M. Rubin, and I. Dubchak.** 2004. VISTA: computational tools for comparative genomics. Nucleic Acids Res. **32:**W273–W279.
9. **Gonczy, P., C. Echeverri, K. Oegema, A. Coulson, S. J. Jones, R. R. Copley, J. Duperon, J. Oegema, M. Brehm, E. Cassin, E. Hannak, M. Kirkham, S. Pichler, K. Flohrs, A. Goessen, S. Leidel, A. M. Alleaume, C. Martin, N. Ozlu, P. Bork, and A. A. Hyman.** 2000. Functional genomic analysis of cell division in C. elegans using RNAi of genes on chromosome III. Nature **408:**331–336.
10. **Gornemann, J., K. M. Kotovic, K. Hujer, and K. M. Neugebauer.** 2005. Cotranscriptional spliceosome assembly occurs in a stepwise fashion and requires the cap binding complex. Mol. Cell **19:**53–63.
11. **Gotzmann, J., C. Gerner, M. Meissner, K. Holzmann, R. Grimm, W. Mikulits, and G. Sauermann.** 2000. hNMP 200: a novel human common nuclear matrix protein combining structural and regulatory functions. Exp. Cell Res. **261:**166–179.
12. **Grey, M., A. Dusterhoft, J. A. Henriques, and M. Brendel.** 1996. Allelism of PSO4 and PRP19 links pre-mRNA processing with recombination and error-prone DNA repair in Saccharomyces cerevisiae. Nucleic Acids Res. **24:**4009–4014.
13. **Grillari, J., P. Ajuh, G. Stadler, M. Löscher, R. Voglauer, W. Ernst, J. Chusainow, F. Eisenhaber, M. Pokar, K. Fortschegger, M. Grey, A. I. Lamond, and H. Katinger.** 2005. SNEV is an evolutionarily conserved splicing factor whose oligomerization is necessary for spliceosome assembly. Nucleic Acids Res. **33:**6868–6883.
14. **Grillari, J., O. Hohenwarter, R. M. Grabherr, and H. Katinger.** 2000. Subtractive hybridization of mRNA from early passage and senescent endothelial cells. Exp. Gerontol. **35:**187–197.
15. **Grillari, J., H. Katinger, and R. Voglauer.** 2006. Aging and the ubiquitinome: traditional and non-traditional functions of ubiquitin in aging cells and tissues. Exp. Gerontol. **41:**1067–1079.
16. **Hamatani, T., M. G. Carter, A. A. Sharov, and M. S. Ko.** 2004. Dynamics of global gene expression changes during mouse preimplantation development. Dev. Cell **6:**117–131.
17. **Hatakeyama, S., M. Yada, M. Matsumoto, N. Ishida, and K. I. Nakayama.** 2001. U box proteins as a new family of ubiquitin-protein ligases. J. Biol. Chem. **276:**33111–33120.

18. **Huang, T. T., and A. D. D'Andrea.** 2006. Regulation of DNA repair by ubiquitylation. Nat. Rev. Mol. Cell Biol. **7:**323–334.
19. **Jumaa, H., G. Wei, and P. J. Nielsen.** 1999. Blastocyst formation is blocked in mouse embryos lacking the splicing factor SRp20. Curr. Biol. **9:**899–902.
20. **Jurica, M. S., and M. J. Moore.** 2003. Pre-mRNA splicing: awash in a sea of proteins. Mol. Cell **12:**5–14.
21. **Kamath, R. S., A. G. Fraser, Y. Dong, G. Poulin, R. Durbin, M. Gotta, A. Kanapin, N. Le Bot, S. Moreno, M. Sohrmann, D. P. Welchman, P. Zipperlen, and J. Ahringer.** 2003. Systematic functional analysis of the Caenorhabditis elegans genome using RNAi. Nature **421:**231–237.
22. **Kortlever, R. M., P. J. Higgins, and R. Bernards.** 2006. Plasminogen activator inhibitor-1 is a critical downstream target of p53 in the induction of replicative senescence. Nat. Cell Biol. **8:**877–884.
23. **Krishnamurthy, J., C. Torrice, M. R. Ramsey, G. I. Kovalev, K. Al-Regaiey, L. Su, and N. E. Sharpless.** 2004. Ink4a/Arf expression is a biomarker of aging. J. Clin. Investig. **114:**1299–1307.
24. **Löscher, M., K. Fortschegger, G. Ritter, M. Wostry, R. Voglauer, J. A. Schmid, S. Watters, A. J. Rivett, P. Ajuh, A. I. Lamond, H. Katinger, and J. Grillari.** 2005. Interaction of U-box E3 ligase SNEV with PSMB4, the β7 subunit of the 20 S proteasome. Biochem. J. **388:**593–603.
25. **Mahajan, K. N., and B. S. Mitchell.** 2003. Role of human Pso4 in mammalian DNA repair and association with terminal deoxynucleotidyl transferase. Proc. Natl. Acad. Sci. USA **100:**10746–10751.
26. **Makarova, O. V., E. M. Makarov, H. Urlaub, C. L. Will, M. Gentzel, M. Wilm, and R. Luhrmann.** 2004. A subset of human 35S U5 proteins, including Prp19, function prior to catalytic step 1 of splicing. EMBO J. **23:**2381–2391.
27. **Mansour, S. L., K. R. Thomas, and M. R. Capecchi.** 1988. Disruption of the proto-oncogene int-2 in mouse embryo-derived stem cells: a general strategy for targeting mutations to non-selectable genes. Nature **336:**348–352.
28. **Milchanowski, A. B., A. L. Henkenius, M. Narayanan, V. Hartenstein, and U. Banerjee.** 2004. Identification and characterization of genes involved in embryonic crystal cell formation during Drosophila hematopoiesis. Genetics **168:**325–339.
29. **Nagy, A., M. Gertsenstein, K. Vintersten, and R. Behringer.** 2003. Manipulating the mouse embryo: a laboratory manual, 3rd ed. Cold Spring Harbor Laboratory Press, Cold Spring Harbor, NY.
30. **Ohi, M. D., and K. L. Gould.** 2002. Characterization of interactions among the Cef1p-Prp19p-associated splicing complex. RNA **8:**798–815.
31. **Ohi, M. D., C. W. Vander Kooi, J. A. Rosenberg, L. Ren, J. P. Hirsch, W. J. Chazin, T. Walz, and K. L. Gould.** 2005. Structural and functional analysis of essential pre-mRNA splicing factor Prp19p. Mol. Cell. Biol. **25:**451–460.
32. **O'Keefe, R. T., A. Mayeda, C. L. Sadowski, A. R. Krainer, and D. L. Spector.** 1994. Disruption of pre-mRNA splicing in vivo results in reorganization of splicing factors. J. Cell Biol. **124:**249–260.
33. **Parrinello, S., E. Samper, A. Krtolica, J. Goldstein, S. Melov, and J. Campisi.** 2003. Oxygen sensitivity severely limits the replicative lifespan of murine fibroblasts. Nat. Cell Biol. **5:**741–747.
34. **Sibilia, M., and E. F. Wagner.** 1995. Strain-dependent epithelial defects in mice lacking the EGF receptor. Science **269:**234–238.
35. **Smith, T. F., C. Gaitatzes, K. Saxena, and E. J. Neer.** 1999. The WD repeat: a common architecture for diverse functions. Trends Biochem. Sci. **24:**181–185.
36. **Tanackovic, G., and A. Kramer.** 2005. Human splicing factor SF3a, but not SF1, is essential for pre-mRNA splicing in vivo. Mol. Biol. Cell **16:**1366–1377.
37. **Todaro, G. J., and H. Green.** 1963. Quantitative studies of the growth of mouse embryo cells in culture and their development into established lines. J. Cell Biol. **17:**299–313.
38. **Urano, Y., M. Iiduka, A. Sugiyama, H. Akiyama, K. Uzawa, G. Matsumoto, Y. Kawasaki, and F. Tashiro.** 2006. Involvement of the mouse Prp19 gene in neuronal/astroglial cell fate decisions. J. Biol. Chem. **281:**7498–7514.
39. **Voglauer, R., M. W. Chang, B. Dampier, M. Wieser, K. Baumann, T. Sterovsky, M. Schreiber, H. Katinger, and J. Grillari.** 2006. SNEV overexpression extends the life span of human endothelial cells. Exp. Cell Res. **312:**746–759.
40. **Wang, B. B., and V. Brendel.** 2004. The ASRG database: identification and survey of Arabidopsis thaliana genes involved in pre-mRNA splicing. Genome Biol. **5:**R102.
41. **Wang, H. Y., X. Xu, J. H. Ding, J. R. Bermingham, Jr., and X. D. Fu.** 2001. SC35 plays a role in T cell development and alternative splicing of CD45. Mol. Cell **7:**331–342.
42. **Wang, J., Y. Takagaki, and J. L. Manley.** 1996. Targeted disruption of an essential vertebrate gene: ASF/SF2 is required for cell viability. Genes Dev. **10:**2588–2599.
43. **Zeng, F., D. A. Baldwin, and R. M. Schultz.** 2004. Transcript profiling during preimplantation mouse development. Dev. Biol. **272:**483–496.
44. **Zhang, N., R. Kaur, X. Lu, X. Shen, L. Li, and R. J. Legerski.** 2005. The Pso4 mRNA splicing and DNA repair complex interacts with WRN for processing of DNA interstrand cross-links. J. Biol. Chem. **280:**40559–40567.